Science Advances

AAAS

advances.sciencemag.org/cgi/content/full/3/11/eaaq0723/DC1

Supplementary Materials for

Synthetic "smart gel" provides glucose-responsive insulin delivery in diabetic mice

Akira Matsumoto, Miyako Tanaka, Hiroko Matsumoto, Kozue Ochi, Yuki Moro-oka, Hirohito Kuwata, Hironori Yamada, Ibuki Shirakawa, Taiki Miyazawa, Hitoshi Ishii, Kazunori Kataoka, Yoshihiro Ogawa, Yuji Miyahara, Takayoshi Suganami

Published 22 November 2017, *Sci. Adv.* **3**, eaaq0723 (2017)
DOI: 10.1126/sciadv.aaq0723

This PDF file includes:

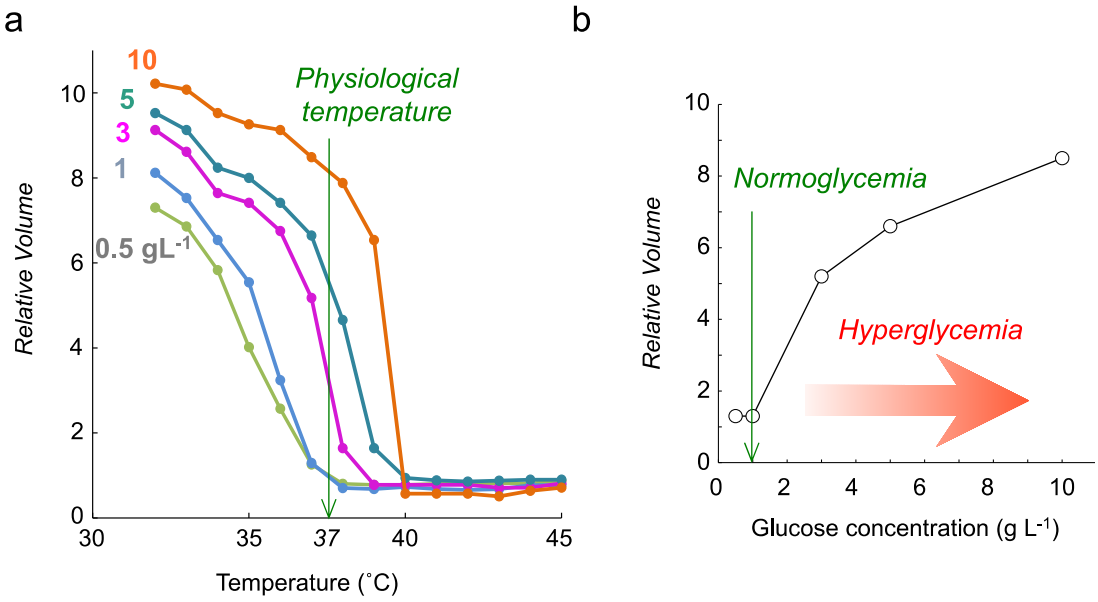

fig. S1. Phase diagram of the gel. a) Phase diagram of the gel showing the equilibrium volume changes as a function of temperature for various glucose concentrations investigated at pH 7.4. The green arrow indicates physiological temperature (37 °C). b) Equilibrium volume change of the gel as a function of the glucose concentration at 37 °C. The green arrow indicates the normoglycemic concentration of glucose (100 mg/dl). Data shown is partially modified from reference 18.

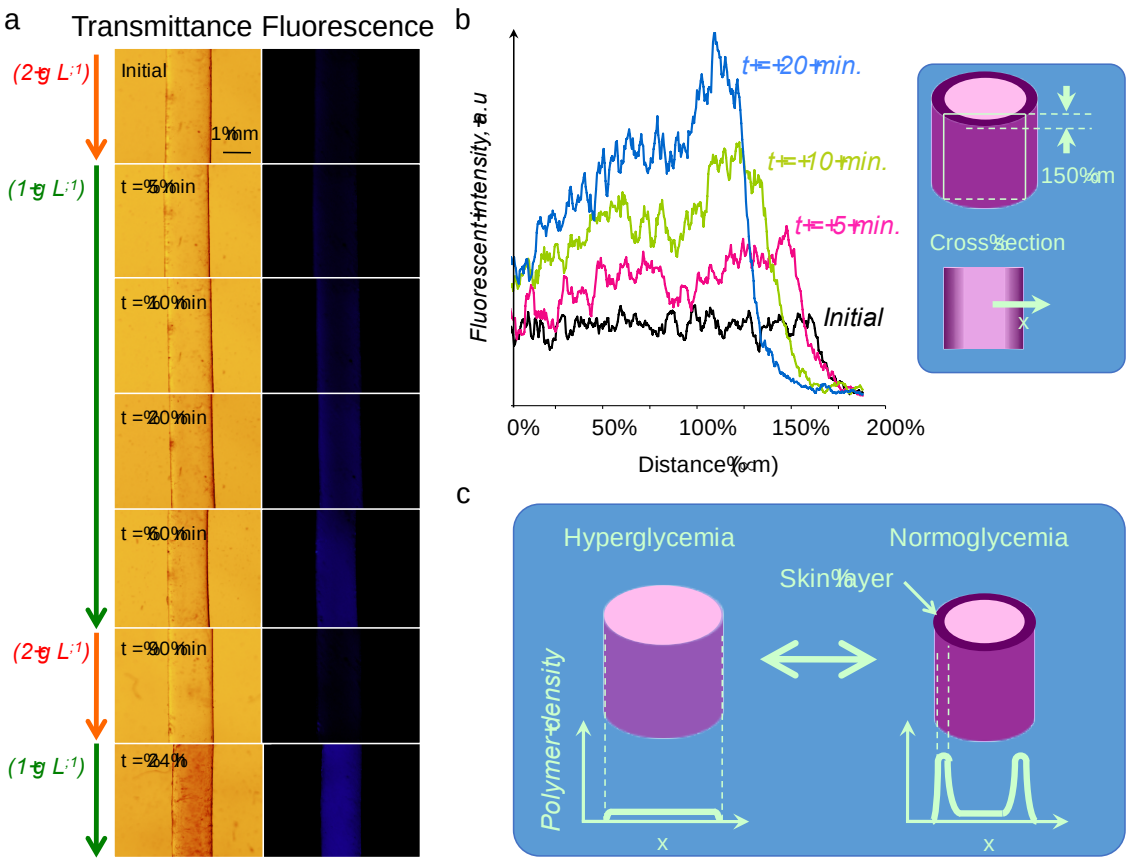

fig. S2. Assessment of skin layer formation. a) Time-course (left) transmittance and (right) 8-anilino-1-naphthalene sulfonic acid (ANS) fluorescence top-view images of a cylinder-shaped piece of gel when changing the glucose concentration under pH 7.4 and 37 °C. Indicated in each transmittance image are the elapsed times after the initial lowering of the concentration from 200 mg/dl to 100 mg/dl. In the fluorescence images, the appearance of the skin layer is seen as an increase in the intensity of the blue color of ANS correlating with the dehydration on the gel surface. Conversely, a reduction in the intensity upon an increase of the glucose concentration (t=90 min.) is indicative of the disappearance of the skin layer. b) Changes in the ANS intensity profiles of a 150 μm depth cross-section (from the gel surface) during the growth of the skin layer. c) Schematic representation of the cross-section density distribution of the polymer network in the gel when reversibly forming the skin layer. Data shown is partially modified from reference18.

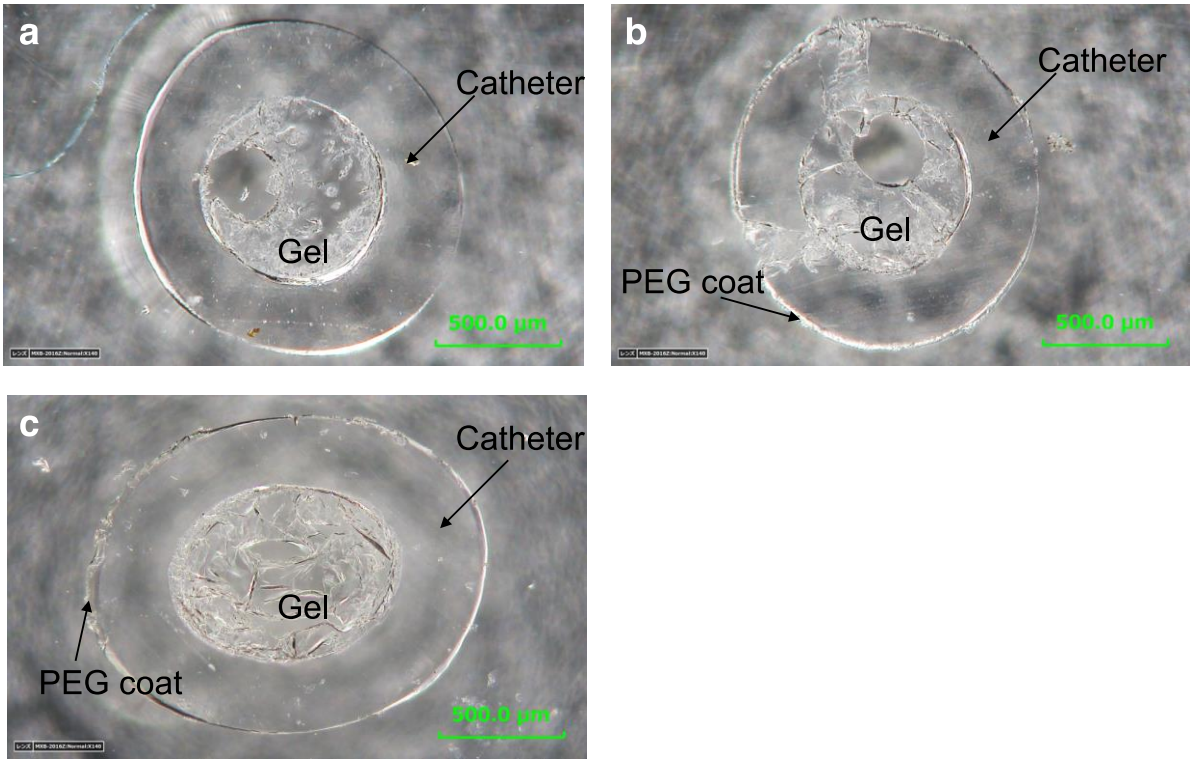

fig. S3. Optical images of the device sections. A comparative analysis of the section in the course of preparation and usage; a. before PEG coating, b. after PEG coating and c. after one week *in vivo* usage of b.

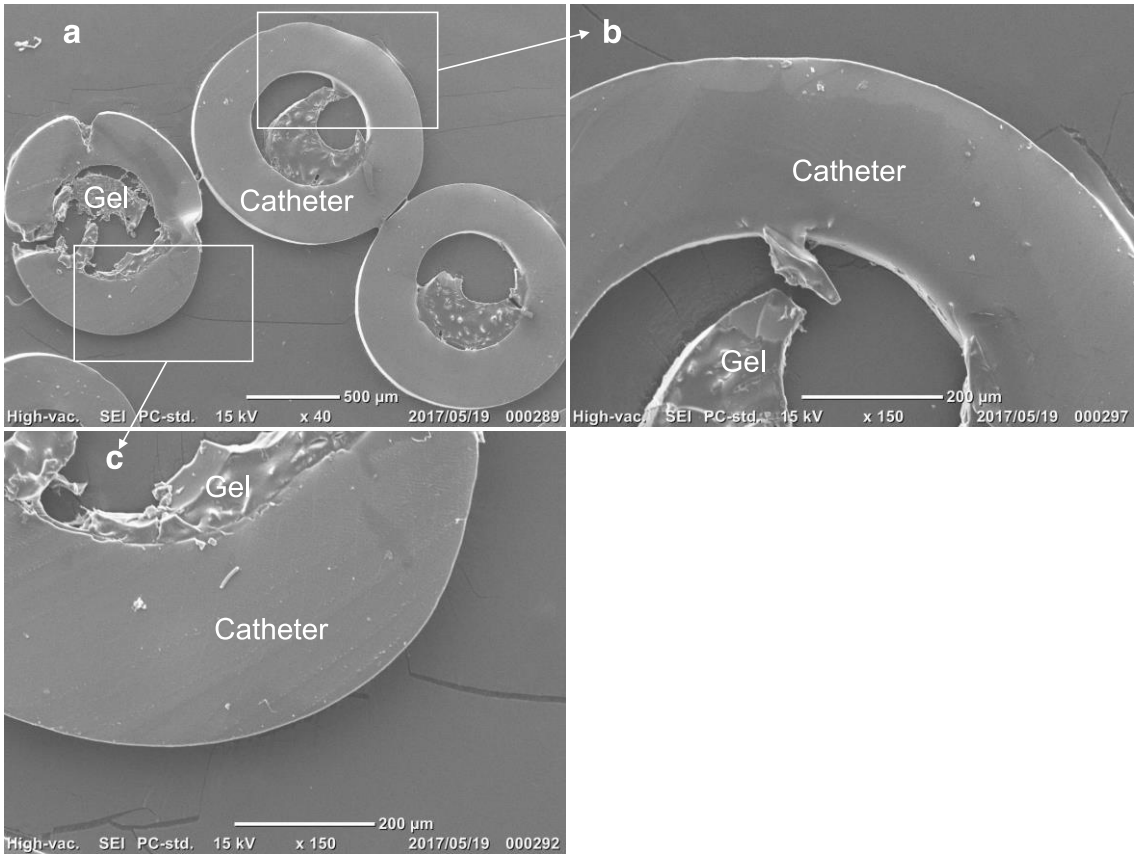

fig. S4. SEM images of the device sections without poly(ethyleneglycol) coating. a. Overview with lower magnification. b,c. Higher-magnification images of the areas indicated in a. Deformation of gel layer was caused during cryo-microtome process, which was absent before the treatment.

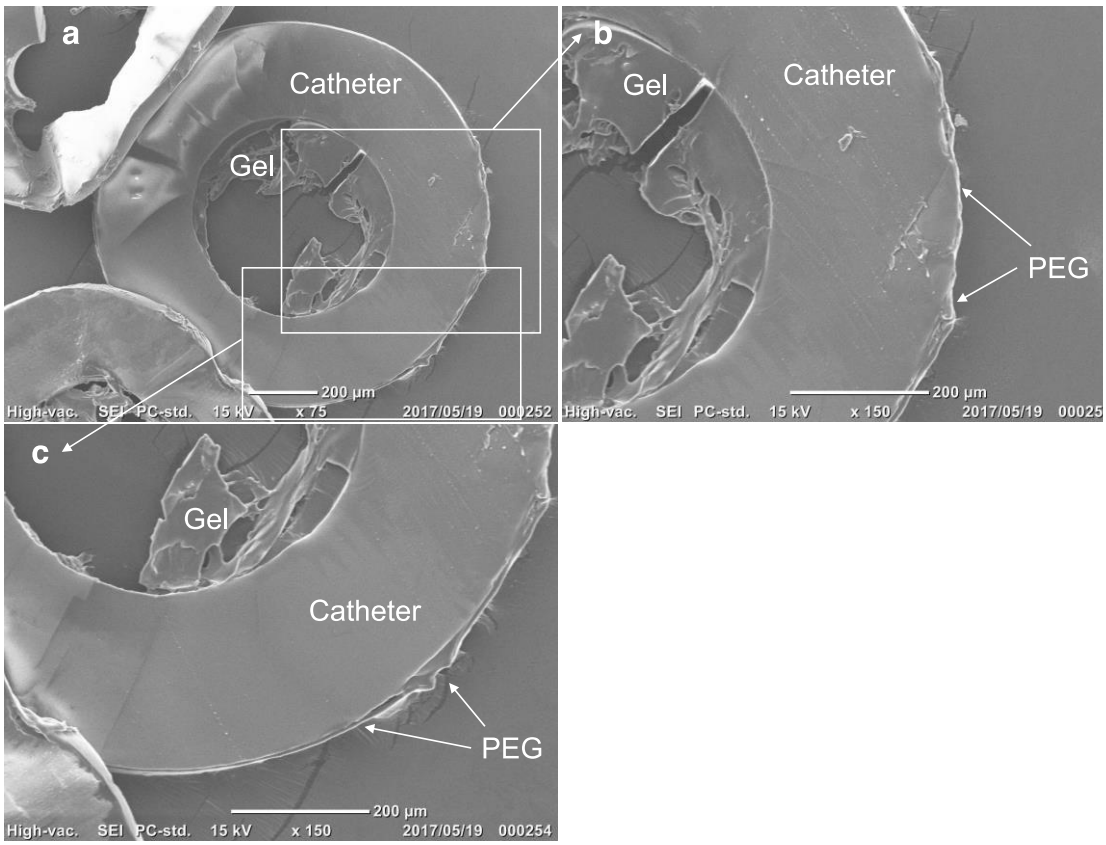

fig. S5. SEM images of the device sections with poly(ethyleneglycol) coating. a. Overview with lower magnification. b,c. Higher-magnification images of the areas indicated in a. Deformation of gel layer was caused during cryo-microtome process, which was absent before the treatment.

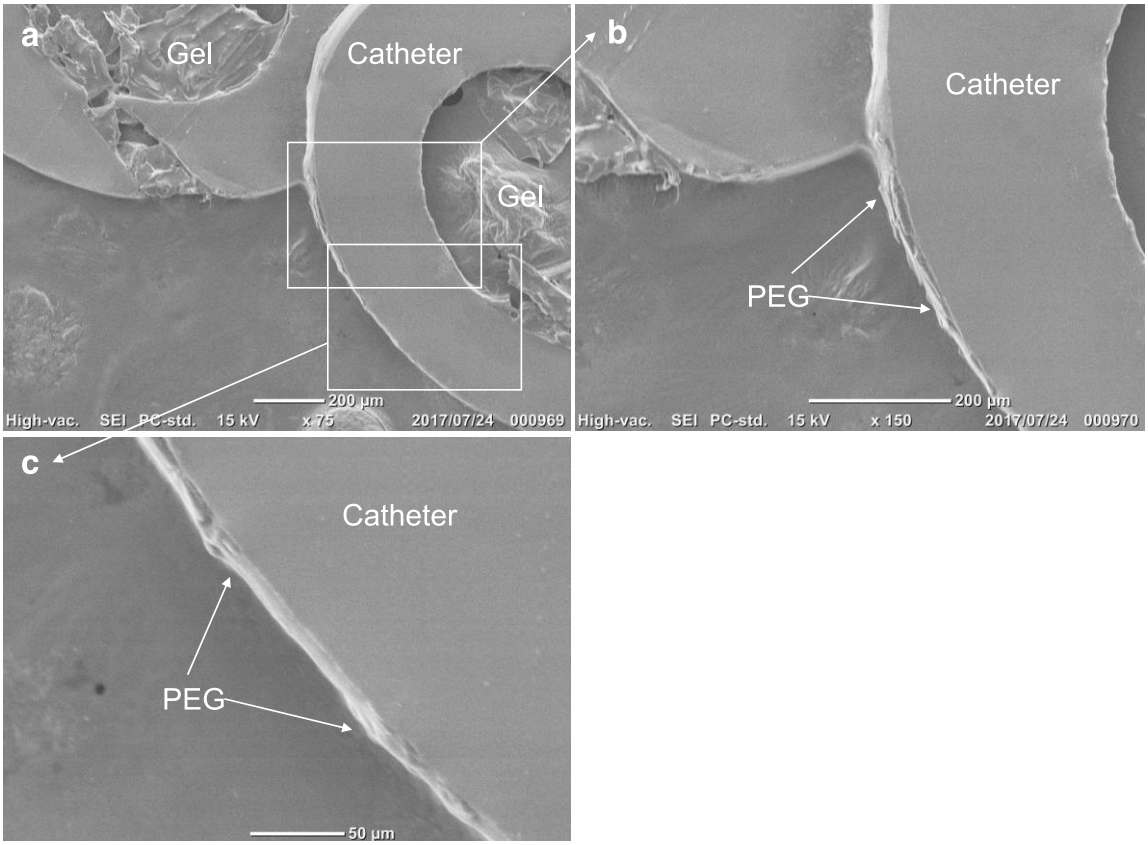

fig. S6. SEM images of the poly(ethyleneglycol)-coated device sections after 1 week in vivo implantation. a. Overview with lower magnification. b,c. Higher-magnification images of the areas indicated in a. Deformation of gel layer was caused during cryo-microtome process, which was absent before the treatment.

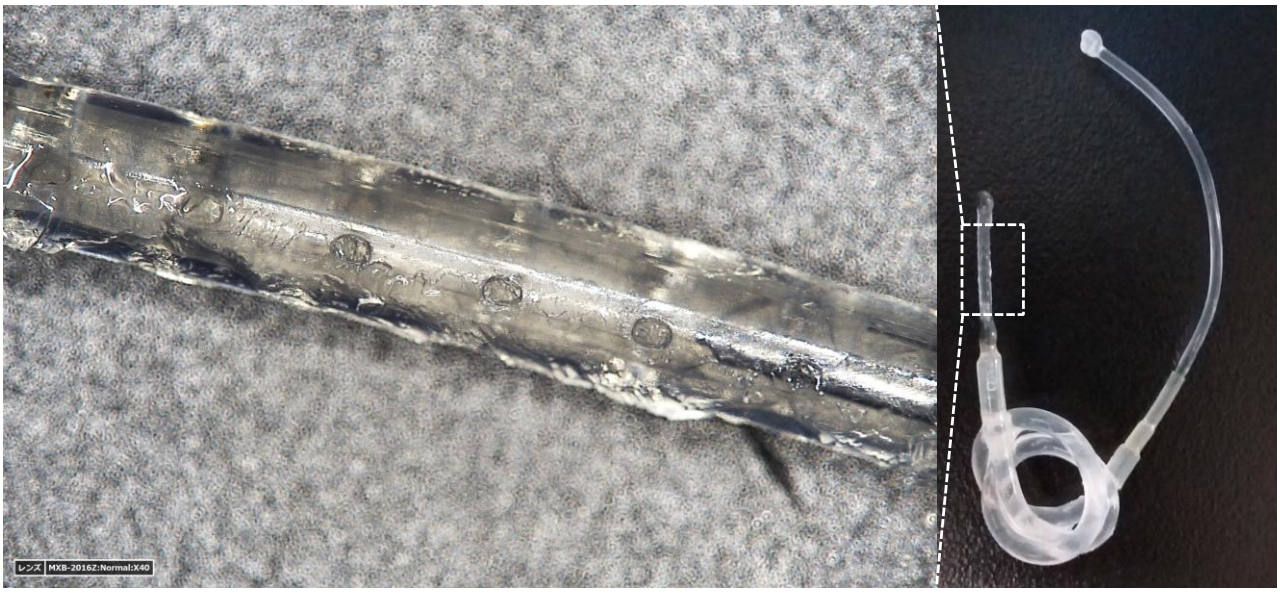

fig. S7. Optical images of the device after 1 week in vivo implantation. (*Left*) Closer look at the gel-modified area. (*Right*) Overview image.

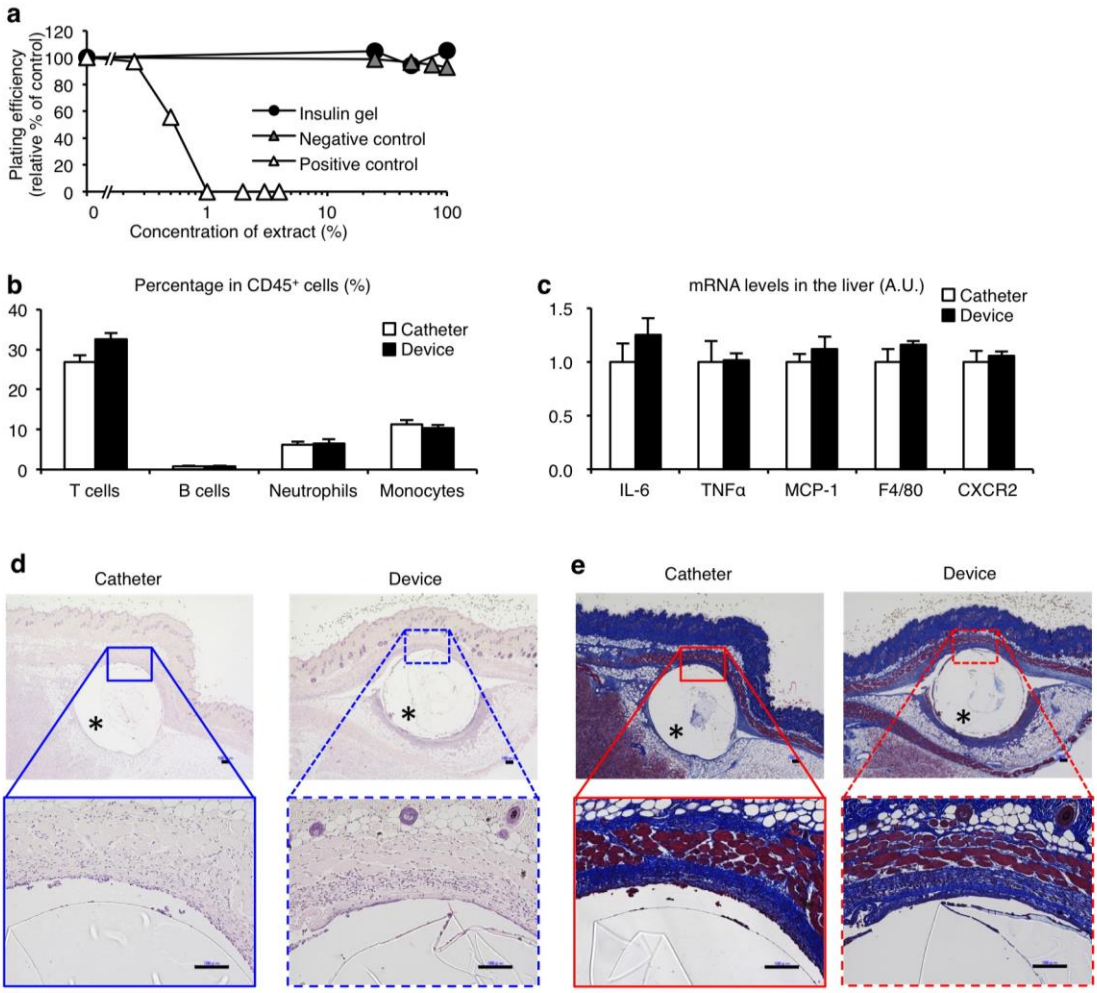

fig. S8. Investigation of biosafety of the device in vitro and in vivo. a. Investigation of biosafety of the device using colony-formation assay *in vitro*. The plating efficiencies of V79 cells cultured with the medium extract of the device and positive and negative control materials. $n = 3$. b-e. Investigation of biosafety of the device using normoglycemic mice *in vivo*. The population of circulating immune cells (b) and mRNA expression in the liver (c) were examined 1 week after the implantation of the device. Representative images of the device and the surrounding subcutaneous tissue stained with hematoxylin and eosin (d) and Masson's Trichrome staining (e). Asterisks indicate silicone catheters. Scale bars, 100 μm. $n = 4$.

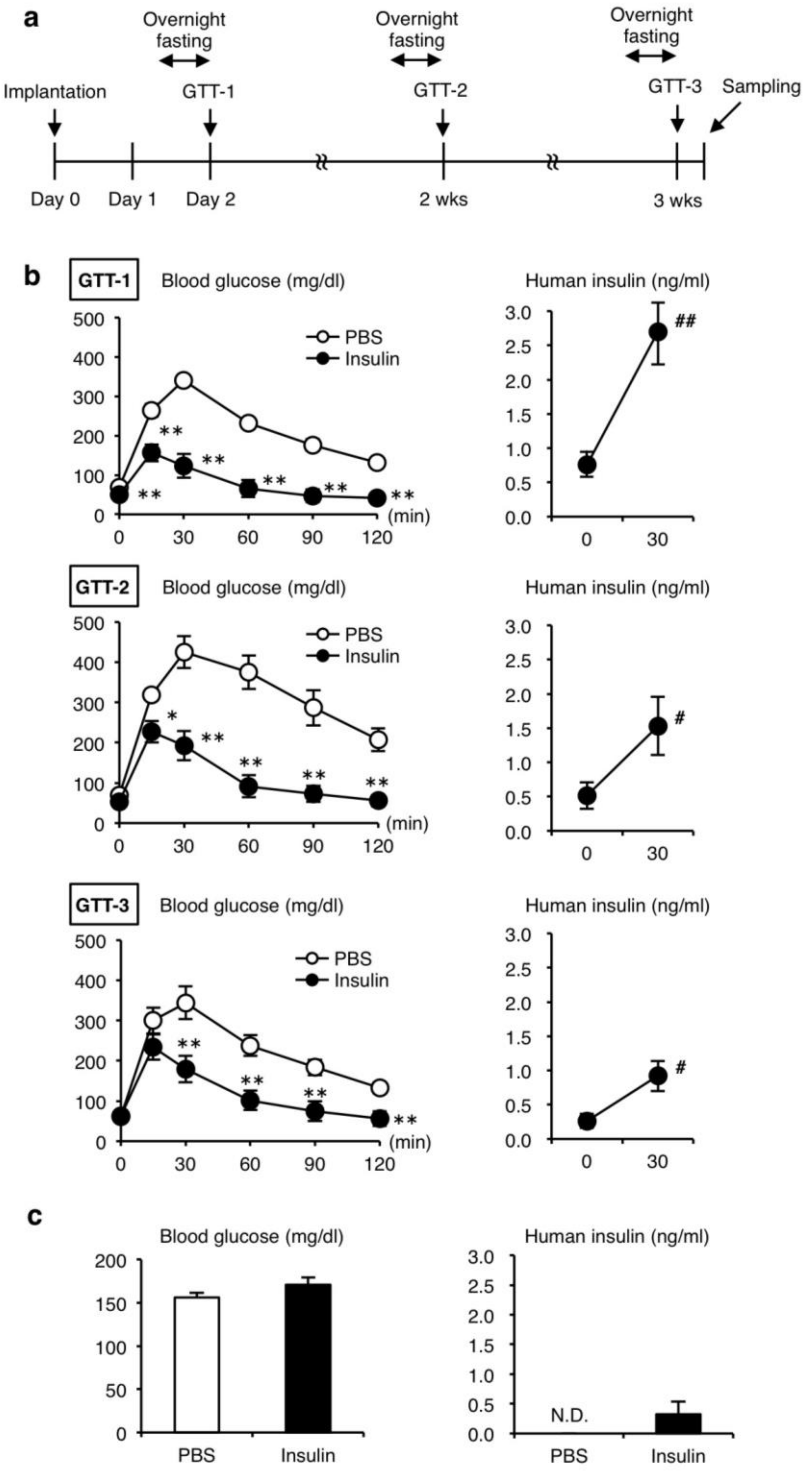

fig. S9. Evaluation of long-term efficacy of the device in vivo. a. Protocol of the experimental design using healthy mice. b. The glucose tolerance test (GTT) (2 g/kg body weight) was performed 2 days, 2 weeks and 3 weeks after the implantation of the device. $^{**}P < 0.01$, $^{*}P < 0.05$ vs. PBS gel group. $^{\#\#}P < 0.01$, $^{\#}P < 0.05$ vs. 0 min. $n = 6$. c. Blood glucose and serum human insulin concentrations under *ad lib*-fed conditions.

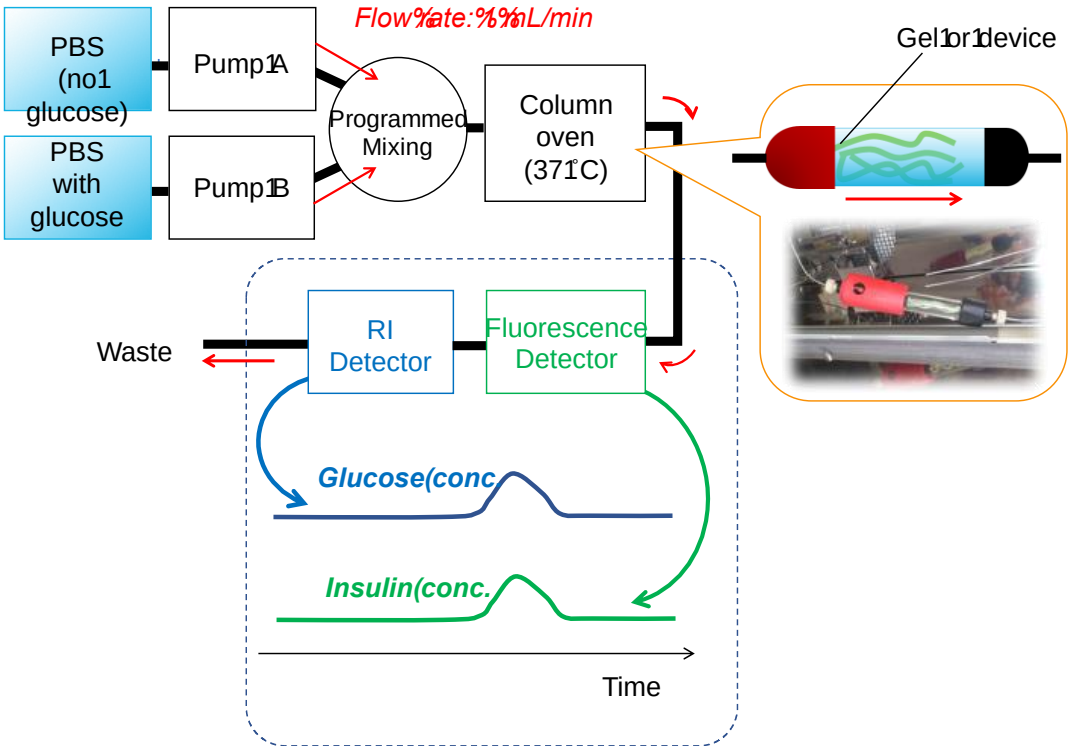

fig. S10. Diagram of the HPLC setup used for release experiments. A HPLC system equipped with two pumps and internal detectors for refractive index (RI) for determination of glucose concentration and fluorescence intensities for determination of FITC-labelled insulin concentration.